

# Out-of-plane momentum and symmetry dependent superconducting gap in $\text{Ba}_{0.6}\text{K}_{0.4}\text{Fe}_2\text{As}_2$

Y. Zhang<sup>1</sup>, L. X. Yang<sup>1</sup>, F. Chen<sup>1</sup>, B. Zhou<sup>1</sup>, X. F. Wang<sup>2</sup>, X. H. Chen<sup>2</sup>, M. Arita<sup>3</sup>,  
K. Shimada<sup>3</sup>, H. Namatame<sup>3</sup>, M. Taniguchi<sup>3</sup>, J. P. Hu<sup>4</sup>, B. P. Xie<sup>1</sup>, D. L. Feng<sup>1\*</sup>

<sup>1</sup> State Key Laboratory of Surface Physics, Department of Physics,  
and Advanced Materials Laboratory, Fudan University, Shanghai 200433, People's Republic of China

<sup>2</sup> Department of Physics, University of science and technology of China,  
Hefei, Anhui 230027, People's Republic of China

<sup>3</sup> Hiroshima Synchrotron Radiation Center and Graduate School of Science,  
Hiroshima University, Hiroshima 739-8526, Japan. and

<sup>4</sup> Department of Physics, Purdue University, West Lafayette, IN 47907, USA

(Dated: June 22, 2010)

The three-dimensional band structure and superconducting gap of  $\text{Ba}_{0.6}\text{K}_{0.4}\text{Fe}_2\text{As}_2$  are studied with high-resolution angle-resolved photoemission spectroscopy. In contrast to previous results, we have identified three hole-like Fermi surfaces near the zone center with sizable out-of-plane or  $k_z$  dispersion. The superconducting gap on certain Fermi surface shows significant  $k_z$ -dependence. Moreover, we found that the superconducting gap sizes are different at the same Fermi momentum for two bands with different spatial symmetries (one odd, one even). Our results further reveal the rich superconducting gap structure in iron pnictides, and provide a distinct test for theories.

The discovery of high- $T_c$  superconductivity in the iron pnictides ignites extensive studies on these materials. However, the pairing symmetry of the superconductivity is still not settled. Most of the present theories propose a  $s_{\pm}$  nodeless order parameter that changes sign between the hole and electron Fermi pockets [1, 2]. However, there are conflicting experimental evidence for the presence of nodes and nodeless superconducting gaps [3, 4]. Furthermore, multiple gap behavior with the gap values varying from  $2\Delta/k_B T_c \approx 1.6$  to 10 has been reported [5, 6]. One possible cause of these controversies is the multi-band nature of iron-based superconductors. In contrast to cuprates, all the five Fe  $3d$  orbitals in iron-based superconductors participate in the low-lying electronic structure, giving a few hole pockets at the zone center and electron pockets at the zone corner [7, 8]. The importance of the Fermi surface topology and their orbital characters has been pointed out by the recent theories [9, 10]. It is proposed that the presence of node is determined by the number of bands which cross the Fermi level, and there are strong anisotropy and amplitude variation of the superconducting gaps on different Fermi surfaces. Moreover, various physical properties of the iron-based superconductors are more three-dimensional (3D) than the cuprates. For example, the isotropy of the upper critical field has been found in  $\text{Ba}_{1-x}\text{K}_x\text{Fe}_2\text{As}_2$  [11].

Previous angle-resolved photoemission spectroscopy (ARPES) studies show isotropic nodeless gaps on all the Fermi surfaces in  $\text{Ba}_{1-x}\text{K}_x\text{Fe}_2\text{As}_2$  [12, 13],  $\text{BaFe}_{2-y}\text{Co}_y\text{As}_2$  [14], and  $\text{Fe}_{1.03}\text{Te}_{0.7}\text{Se}_{0.3}$  [15]. The most representative and detailed data to date were taken on the optimally doped  $\text{Ba}_{1-x}\text{K}_x\text{Fe}_2\text{As}_2$  samples with a  $T_c$  of 38 K. Two hole pockets were observed near the zone

center, and the superconducting gap on the inner hole pocket is found to be larger than that on the outer pocket, which is consistent with the prediction of theories of  $s_{\pm}$  pairing symmetry with a gap function proportional to  $|\cos k_x \cos k_y|$ . However, there are still many issues to be resolved. For example, band calculations predict three hole Fermi surface sheets at the zone center rather than two. The relationship between orbital characters and superconducting gaps is yet to be established. Furthermore, band calculation suggested that the 3D characters of the electronic structure are important for the magnetism and superconductivity in the iron-based superconductors [16]. But due to the limited photon energies used in previous ARPES studies, the superconducting gap behavior along the out-of-plane momentum ( $k_z$ ) direction has not been exposed. The resolutions of these issues are important to the understanding of the superconducting pairing mechanism in iron-based superconductors.

In this Letter, we have studied the  $k_z$  dependence of the superconducting gap in high quality  $\text{Ba}_{0.6}\text{K}_{0.4}\text{Fe}_2\text{As}_2$  single crystals with ARPES. We found that the Fermi surface near the zone center  $\Gamma$  actually contains three hole pockets instead of two as previously reported. By changing the photon energy, we have revealed the 3D character of the electronic structure and the superconducting gaps. Significant  $k_z$  dependence of the superconducting gap is discovered on one of the bands. Particularly, we found that at the same momentum, bands with different symmetries could exhibit very different gap sizes. Our results provide a more global picture of the gap in the material, which would help the construction of microscopic models of the iron-based superconductors.

High quality  $\text{Ba}_{0.6}\text{K}_{0.4}\text{Fe}_2\text{As}_2$  ( $T_c = 38$  K) single crystals were synthesized by self-flux method [17] with a superconducting transition width of 0.5 K. Data were taken with various photon energies at the Beamline 5-4 of Stanford Synchrotron Radiation Laboratory (SSRL), and

---

\*Electronic address: dlffeng@fudan.edu.cn

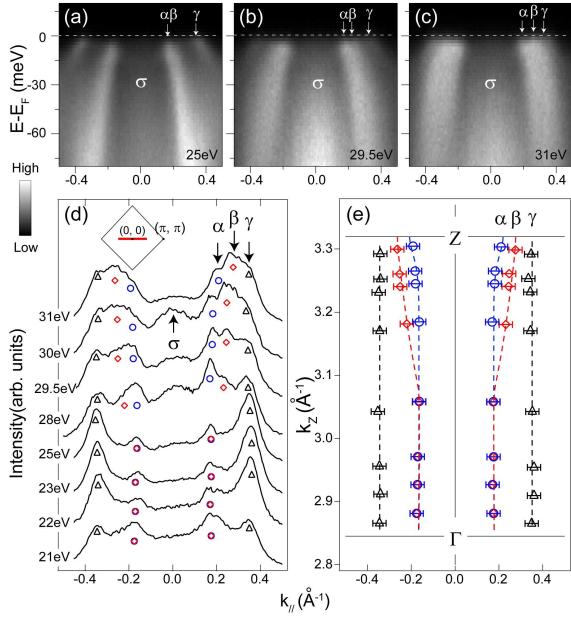


FIG. 1: (color online) (a), (b), and (c) Photoemission data of  $\text{Ba}_{0.6}\text{K}_{0.4}\text{Fe}_2\text{As}_2$  along the  $(0, 0)-(\pi, \pi)$  direction taken with 25, 29.5, and 31 eV respectively. (d) The MDCs at  $E_F$  taken with different photon energies are stacked. The inset shows the projection of the cuts in the 2D Brillouin zone. (e) The  $k_F$ 's determined from the MDCs in panel d. Data were taken at 10 K.

with 21.2 eV Helium-I $\alpha$  line of a discharge lamp in mixed polarization geometry. Polarization dependent data were taken at the Beamline 1 of Hiroshima synchrotron radiation center (HSRC). Two polarization geometries ( $E_p$ ,  $E_s$ ) were achieved by rotating the experimental chamber. All the data were taken with Scienta electron analyzers, the overall energy resolution is 15 meV at HSRC or 7 meV at SSRL, and angular resolution is 0.3 degree. The samples were cleaved *in situ*, and measured under ultra-high-vacuum of  $5 \times 10^{-11}$  torr.

Since the superconducting gap is almost isotropic around the Fermi surface cross-section of certain  $k_z$  [12, 13], we would focus on the  $k_z$  dependence of the superconducting gaps along the  $(0, 0)-(\pi, \pi)$  high symmetry cut for simplicity. The photon energy dependent data are shown in Fig. 1. Only two bands could be resolved in 25 eV [Fig. 1(a)], forming two hole pockets as observed in previous studies. However, by changing the photon energy, we could observe an additional bands ( $\beta$ ) moving outwards with 29.5 eV and 31 eV photons [Fig. 1(b) and 1(c)]. The Fermi momenta ( $k_F$ ) of these three bands are determined by peak positions in momentum distribution curves (MDCs) at the Fermi energy ( $E_F$ ) [18] in Fig. 1(d). Taking the inner potential of 15 eV [19] to calculate the  $k_z$ 's of different photon energies, our data cover half of the Brillouin zone along  $k_z$  direction from  $\Gamma$  with  $\sim 21$  eV photons to  $Z$  with  $\sim 31$  eV photons [Fig. 1(e)]. The  $\alpha$  and  $\gamma$  bands show little  $k_z$  dispersion, while  $\beta$  is almost degenerate with  $\alpha$  near  $\Gamma$ , but moves outward significantly

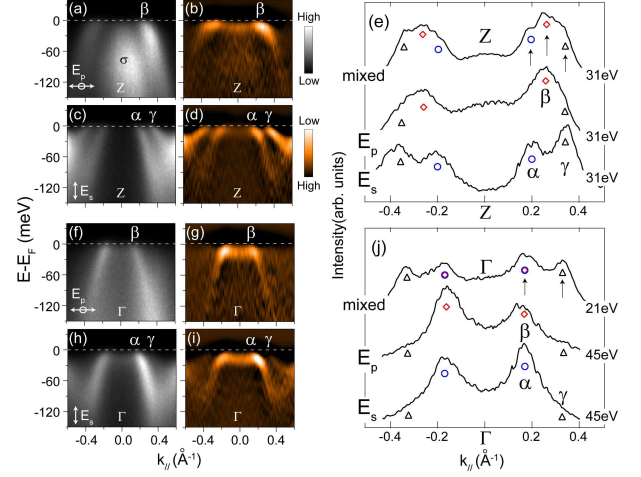


FIG. 2: (color online) (a) Photoemission intensity near  $Z$  along the  $(0, 0)-(\pi, \pi)$  direction taken in the  $E_p$  geometry with 31 eV photons. (b) The second derivative with respect to energy of data in panel a. (c) and (d) are the same as panels a and b respectively but taken in the  $E_s$  geometry. (e) The MDCs at  $E_F$  with mixed,  $E_p$ , and  $E_s$  polarization geometries near  $Z$ . (f), (g), (h), and (i) are the same as panels a, b, c, and d respectively but taken with 45 eV photons to reach the  $\Gamma$  point. (j) The MDCs at  $E_F$  with mixed,  $E_p$ , and  $E_s$  polarization geometries near  $\Gamma$ . Data were taken at 40 K.

near  $Z$ . Since previous ARPES studies were restricted around the  $\Gamma$  region,  $\alpha$  and  $\beta$  could not be distinguished. Therefore, three bands reported here with distinct  $k_z$  dispersions naturally resolve the previous inconsistency with band structure calculations, which predicted three hole pockets around the zone center [9, 10].

To further reveal the orbital characters of these three bands, we have conducted polarization dependent ARPES experiment. The polarization geometry  $E_p(E_s)$  could be achieved, with the polarization direction parallel (perpendicular) to the mirror plane defined by the sample normal and the  $(0, 0)-(\pi, \pi)$  direction. The orbitals of even (odd) symmetry with respect to the mirror plane could be observed in  $E_p(E_s)$  geometry [20]. The polarization dependent data around  $Z$  are shown in Figs. 2(a)-2(d).  $\beta$  could only be observed in  $E_p$  geometry, thus it has even orbital character. Oppositely,  $\alpha$  only shows up in  $E_s$  geometry, which suggests an odd orbital character.  $\gamma$  mostly has odd orbital character [Figs. 2(c) and 2(d)], but there is also some trace of  $\gamma$  in  $E_p$  geometry due to possible orbital mixing. The MDCs at  $E_F$  of different polarization geometries around  $Z$  are compared in Fig. 2(e). The peak positions in  $E_p$  and  $E_s$  geometry are consistent with the data taken in mixed polarization geometry. Since the different symmetries of  $\alpha$  and  $\beta$  should not change along  $k_z$  [16], it enables us to separate them with polarization dependent experiment around  $\Gamma$ , as shown in Fig. 2(f)-2(i). The MDC peaks of  $\alpha$  and  $\beta$  show up at the same momentum in Fig. 2(j). This agrees well with our photon energy dependent data

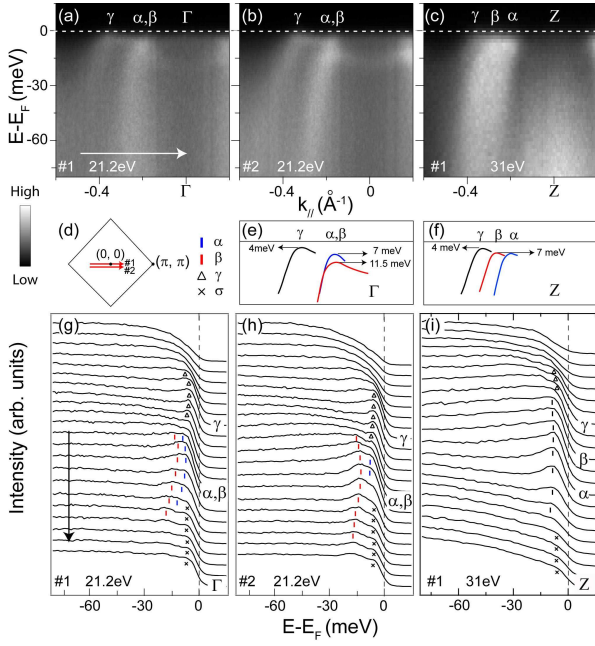


FIG. 3: (color online) (a) and (b) Photoemission intensities taken with 21.2 eV along two momentum cuts as indicated in panel d. (c) is the same as panel a, but taken near Z with 31 eV photon energy. (e) and (f) are cartoons of the bands in panels a and c respectively. (g), (h), and (i) EDCs of the data in panels a, b, and c respectively. Data were taken at 10K.

that the  $k_F$ 's of the  $\alpha$  and  $\beta$  bands are almost degenerate around  $\Gamma$ , but separated from each other around Z. Note that the intensity of  $\gamma$  is very weak in the polarization data around  $\Gamma$  due to possible matrix element effects of the particular photon energy and/or experimental setup.

The two odd and one even bands observed here qualitatively agree with the prediction of the band calculations, where only three orbitals  $d_{xz}$ ,  $d_{yz}$ , and  $d_{xy}$  contribute to the low energy electronic structure around  $\Gamma$  [9, 10]. The  $\beta$  band is  $d_{xz}$  orbital due to its even symmetry. The  $\gamma$  band shows little dispersion along the  $k_z$  direction, which is most likely the  $d_{xy}$  orbital with two-dimensional (2D) character. The  $\alpha$  band is thus assigned to the  $d_{yz}$  orbital, which is predicted to be degenerate with the  $d_{xz}$  orbital at  $\Gamma$  by theory. Note that there are some broad spectral weight ( $\sigma$ ) at  $(0, 0)$ , which is possibly due to the contribution of  $d_{z^2}$  bands below  $E_F$  or the incoherent spectral weight scattered from other states [Figs. 1 and 2(a)]; they are thus ignored in the following discussions.

The data in the superconducting state near  $\Gamma$  are shown in Figs. 3(a) and 3(b). The  $\gamma$  band shows simple Bogoliubov dispersion with an energy gap about 4 meV. Most notably, at the  $k_F$ 's of the  $\alpha$  and  $\beta$  bands, the EDCs exhibit a complex structure with two peaks [Figs. 3(g) and 3(h)]. The peak positions could be tracked towards  $\Gamma$  with Bogoliubov like dispersion of two energy scales (7 meV and 11.5 meV) as shown in Fig. 3(e). The energy scale of 11.5 meV is consistent with the gap size observed

in previous ARPES experiments [12]. Moreover, the clear bending-over behavior and small peak width clearly reproduce the properties of a superconducting peak. Furthermore, the peak at 7 meV should not be the bent-over feature of the  $\gamma$  band, as one can track the  $\gamma$  band by the triangles in Fig. 3(g) and 3(h). It quickly bends over to high binding energies and loses its weight significantly. Therefore, the most natural explanation of our results is that the  $\alpha$  and  $\beta$  bands have different superconducting gaps at the same momentum. On the other hand, while these three bands could be clearly separated around the Z point in Fig. 3(c), only single peak could be observed at the Fermi crossings of  $\alpha$  and  $\beta$  with a superconducting gap of 7 meV [Fig. 3(i)].

In the five-band model, the Fermi surfaces of iron-based superconductors consist of sections with different orbital characters [7, 10]. It has been proposed that the multi-orbital interactions could form strong gap anisotropy on the Fermi surfaces. Therefore, the observation of two energy scales of  $\alpha$  and  $\beta$  could be directly related to their orbital nature, since they show opposite orbital symmetries at the same Fermi momentum position. That is, the pairing strengths could be strongly determined by the orbital symmetries. The next question is which band provides a larger gap around  $\Gamma$ . Considering there is a significant change from 11.5 meV to 7 meV for one of the gaps along the  $k_z$  direction, plus the strong  $k_z$  dependence of  $\beta$ , it is reasonable to assume that the  $\beta$  band contributes to the larger gap of 11.5 meV around  $\Gamma$ . We could not completely exclude the possibility of the  $\alpha$  band at this stage, but this assumption would only affect the gap assignment around  $\Gamma$ , and would not affect the observed  $k_z$  dependence of the superconducting gaps discussed below. Polarization dependent experiments with high resolution in the superconducting state are needed to clarify this point. We leave this for further studies.

The symmetrized EDCs at the  $k_F$ 's of the  $\alpha$ ,  $\beta$ , and  $\gamma$  bands are summarized in Figs. 4(a), 4(b), and 4(c). The two-peak behavior could be only resolved around the  $\Gamma$  region. The superconducting gap values are determined by fitting the peak positions in symmetrized EDCs with the common phenomenological superconducting spectral function as illustrated in Fig. 4(a) [21]. The  $k_z$  dependence of superconducting gaps is shown in Fig. 4(e). The gap sizes of  $\alpha$  and  $\gamma$  are always about 7 and 4 meV respectively, and the gap of  $\beta$  shows strong  $k_z$  dependence from 11.5 to 7 meV. In previous ARPES studies, these gaps around  $\Gamma$  can fit well to  $\Delta_0 |\cos k_x \cos k_y|$  [12–15]. Therefore the superconducting gap should decrease away from the  $(0, 0)$  point. We plot the superconducting gap versus  $|\cos k_x \cos k_y|$  in Fig. 4(g). The  $\alpha$  and  $\gamma$  bands could be well fitted in this relation with  $\Delta_0 \approx 8$  meV as shown by the straight line in Fig. 4(g). However, the large deviation of the  $\beta$  band (highlighted by the shaded region) indicates that the  $k_z$  dependence of the superconducting gap could not be explained by the in-plane Fermi surface size change of the  $\beta$  band. Therefore, the  $k_z$  contribution must be included to describe the

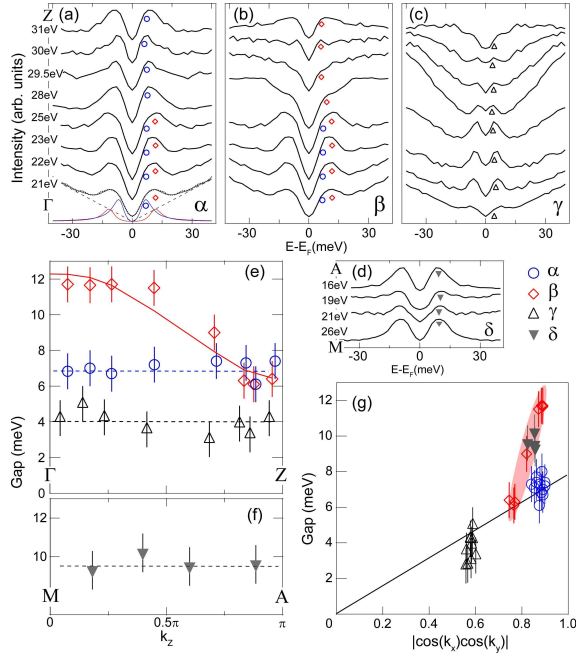


FIG. 4: (a), (b), and (c) Symmetrized EDCs at the  $k_F$ 's of three bands taken with different photon energies. The dashed line in panel a is the background used in the fitting process. (d) Symmetrized EDCs at the momentum  $0.2 \text{ \AA}^{-1}$  from  $(\pi, \pi)$ , which is the  $k_F$  of electron pocket ( $\delta$ ) at the zone corner [12]. (e) and (f)  $k_z$  dependence of the superconducting gaps around the zone center and corner respectively. (g) Gaps vs.  $|\cos k_x \cos k_y|$ .

gap function of the  $\beta$  band. With the simple formula of  $\Delta_{0\beta} |\cos k_x \cos k_y| (1 + A \cos k_z)$ , one can fit the gap of  $\beta$  reasonably well with  $\Delta_{0\beta} \approx 11.2 \text{ meV}$  and  $A \approx 0.24$  as shown by the solid line in Fig 4(e).

The  $k_z$ -dependent superconducting gaps discovered here could not be explained in 2D models, which are used to construct the pairing mechanism in most of previous theories [9, 10]. In contrast to the 2D electronic structure of cuprates, the 3D characters of iron-based superconductors have been highlighted by many properties, *e.g.*,

the small anisotropy of the upper critical field [11, 22], and 3D spin fluctuations in parent and doped compounds [23–25]. Our results further emphasize the 3D character of the superconductivity, where the out-of-plane pairing channels should be considered. Consistently, a substantial  $k_z$  dependence of the superconducting order parameter has been found in a recent 3D band model that is constructed to calculate the spin fluctuations and the pairing function [16].

The superconducting gap size is proposed to relate to the nesting condition of Fermi surfaces between  $\Gamma$  and  $M$  in previous ARPES studies [12, 14]. The Fermi surfaces near the zone corner show weak  $k_z$  dependence [26, 27]. In that case, the change of Fermi surface size of  $\beta$  along  $k_z$  direction could break the nesting condition, and thus significantly change the superconducting gaps. However, it could not explain the different gaps of the  $\alpha$  and  $\beta$  bands, since they have almost the same Fermi surface size around  $\Gamma$ . Moreover, the  $k_z$  dependence of gaps near the zone corner are not so obvious, as shown in Figs. 4(d) and 4(f), and the gap sizes also deviate from the fitting of  $|\cos k_x \cos k_y|$  relation in Figs. 4(g). Therefore, the pairing between  $\Gamma$  and  $M$  could not be just related to simple nesting of the Fermi surfaces. The orbital character and the 3D electronic structure should be taken into account.

To summarize, we have carried out a systematic investigation of the superconducting gap of high quality  $\text{Ba}_{0.6}\text{K}_{0.4}\text{Fe}_2\text{As}_2$  single crystals, and have established a direct connection between the superconductivity and the 3D electronic structure with multi-orbital nature in iron-based superconductors. Our results have set up a more comprehensive picture of the superconducting gap in this compound, which shed new light on the understanding of superconductivity in iron-based superconductors.

We gratefully acknowledge the experimental support by Dr. D. H. Lu and Dr. R.G. Moore at SSRL. This work was supported by the NSFC, MOE, MOST (National Basic Research Program No.2006CB921300), and STCSM of China. SSRL is operated by the US DOE Office of Basic Energy Science.

- 
- [1] I. I. Mazin, *et al.*, Phys. Rev. Lett. **101**, 057003 (2008).
  - [2] Kangjun Seo, B. A. Bernevig, Jiangping Hu, Phys. Rev. Lett. **101**, 206404 (2008).
  - [3] Clifford W. Hicks, *et al.*, Phys. Rev. Lett. **103**, 127003 (2009).
  - [4] T. Y. Chen, *et al.*, Nature (London) **453**, 1224 (2008).
  - [5] T. J. Williams, *et al.*, Phys. Rev. B **80**, 094501 (2009).
  - [6] K. W. Kim, *et al.*, Phys. Rev. B **81**, 214508 (2010).
  - [7] K. Kuroki *et al.*, Phys. Rev. Lett. **101**, 087004 (2009).
  - [8] D. J. Singh and M. H. Du, Phys. Rev. Lett. **100**, 237003 (2008).
  - [9] F. Wang, H. Zhai, D. H. Lee, Phys. Rev. B **81**, 184512 (2010).
  - [10] Ronny Thomale, *et al.*, arXiv:1002.3599. (2010).
  - [11] H. Q. Yuan, *et al.*, Nature (London) **457**, 565 (2009).
  - [12] K. Nakayama, *et al.*, Euro. Phys. Lett. **85**, 67002 (2009).
  - [13] L. Wray *et al.*, Phys. Rev. B **78**, 184508 (2008).
  - [14] K. Terashima, *et al.*, proceedings of the National Academy of Sciences of the USA (PNAS) **106**, 7330-7333 (2009).
  - [15] K. Nakayama, *et al.*, arXiv:0907.0763. (2009).
  - [16] S. Graser, *et al.*, arXiv:1003.0133. (2010).
  - [17] X. F. Wang, *et al.*, Phys. Rev. Lett. **102**, 117005 (2009).
  - [18] A. Kaminski, *et al.*, Phys. Rev. Lett. **86**, 1070 (2001).
  - [19] P. Vilmercati, *et al.*, Phys. Rev. B **79**, 220503(R) (2009).
  - [20] For the detailed description of the selection rules in the different experimental geometries, see Y. Zhang *et al.*, arXiv:0904.4022 (2009).

- [21] M. R. Norman, *et al.*, Phys. Rev. B. **57**, R11093 (1998).
- [22] Minghu. Fang, *et al.*, Phys. Rev. B **81**, 020509(R) (2010).
- [23] Zhao, J. *et al.*, Phys. Rev. Lett. **101**, 167203 (2008).
- [24] R. J. McQueeney, *et al.*, Phys. Rev. Lett. **101**, 227205 (2008).
- [25] Songxue Chi, *et al.*, Phys. Rev. Lett. **102**, 107006 (2009).
- [26] Walid Malaeb, *et al.*, J. Phys. Soc. Jpn. **78**, 123706 (2009).
- [27] C. Liu, *et al.*, Phys. Rev. Lett. **102**, 167004 (2009).